IGARSS 2024 - 2024 IEEE International Geoscience and Remote Sensing Symposium | 979-8-3503-6032-5/24/$31.00 ©2024 IEEE | DOI: 10.1109/IGARSS53475.2024.10641029

# SPARSITY REGULARIZED RANK-$(L, M, N)$ BLOCK TERM DECOMPOSITION FOR HYPERSPECTRAL IMAGE MIXED NOISE REMOVAL

*Hao Zhang*[†], *Ting-Zhu Huang* [†*], *Jie Lin* [†], *Tai-Xiang Jiang* [‡]

[†]School of Mathematical Sciences, University of Electronic Science and Technology of China
[‡]School of Computing and Artificial Intelligence, Southwestern University of Finance and Economics

## ABSTRACT

Tensor decomposition-based models have received increasing attention in hyperspectral image (HSI) denoising. However, tensor decompositions (e.g., Tucker decomposition and tensor singular value decomposition) in these HSI denoising models ignore exploiting the multiple components of the HSI, resulting in unsatisfactory denoising performance. To fully exploit the multiple components of the HSI, we develop a sparsity regularized rank-$(L, M, N)$ block term decomposition (SR-BTD). In SR-BTD, the clean HSI is decomposed as the sum of multiple components, where each component is a sparse core tensor multiplied by matrices along each mode. The sparse regularization on each core tensor can benefit determining the low-rankness of each component with the unknown rank-$(L, M, N)$ in the real world, leading to more accurately exploiting each component. Equipped with SR-BTD, we establish the HSI denoising model and design a hierarchical alternating least squares-based algorithm to efficiently solve the resulting model. Extensive experiments on simulated and real HSI denoising tasks demonstrate SR-BTD is superior to the competing tensor decompositions in terms of numerical results and visual quality.

***Index Terms*—** Tensor, block term decomposition, mixed noise removal, hyperspectral images.

## 1. INTRODUCTION

Hyperspectral images (HSIs) denoising aims at improving the quality of the corrupted HSIs for the segmentation [1], matching [2], classification [3], and spectral signature unmixing [4]. Different from gray-scale or RGB images, the noise in HSIs complex consists of Gaussian noise, impulse noise, stripes, and deadlines [5, 6]. Therefore, HSI denoising is challenging and has received increasing attention.

The strong spatial and spectral correlation of the HSI provides possibility for the HSI denoising. One important prior to characterizing the spatial and spectral correlation of the HSI is the low-rankness. Some classical HSI denoising methods are based on the matrix low-rankness, where the HSI is unfolded along the third mode [7–10]. However, unfolding the HSI to the matrix will destroy the intrinsic structure.

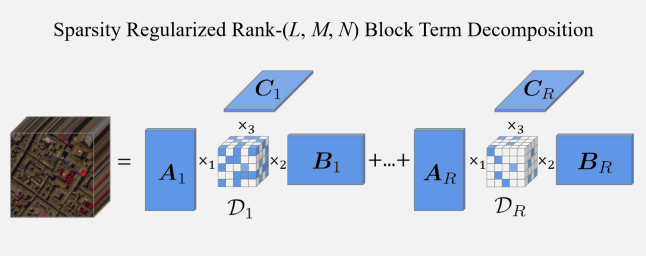


**Fig. 1**: The flowchart of the proposed sparsity regularized rank-$(L, M, N)$ block term decomposition of the HSI. Here, the HSI is decomposed as a sum of multiple components, where each component is a sparse core tensor (i.e, $\mathcal{D}_r$) multiplied by matrices (i.e., $\boldsymbol{A}_r$, $\boldsymbol{B}_r$, and $\boldsymbol{C}_r$) along each mode.

Since an HSI is naturally a three-way tensor, tensor decomposition-based models are considered to exploit the low-rankness of the HSI for denoising task [11]. There are different tensor decompositions introduced in the HSI denoising model. Tucker decomposition, which is a classical strategy, decomposes a tensor into a core tensor multiplied by matrices along each mode [12]. There are many HSI denoising models inspired by the Tucker decomposition like LRTA [12], GKTD [13], and LRTDTV [14]. To address the dimensional curse of the Tucker decomposition, tensor network decompositions, including tensor train (TT) decomposition and tensor ring (TR) decomposition, have been developed [15, 16], which decompose the tensor into several low-dimensional tensor/matrix factors. Additionally, a new tensor singular value decomposition (T-SVD) is introduced in HSI denoising [17]. T-SVD decomposes a tensor as two orthogonal tensors and one $f$-diagonal tensor [18]. Fan *et al.* introduced T-SVD and spatial-spectral total variation for the HSI recovery [19]. Zheng *et al.* developed T-SVD to 3D-TSVD to exploit the correlation of different modes of the HSI [20]. In summary, these reviewed tensor decompositions mainly characterize the global correlation of the HSI.

However, only exploiting the global correlation can not accurately characterize the HSI. From the unmixing aspect,

*Corresponding author: tingzhuhuang@126.com. This research is supported by NSFC (No. 12171072), National Key Research and Development Program of China (No. 2020YFA0714001).

HSI physically reflects the abundance of different matters, which means HSI has multiple components. Recently, the block term decomposition (BTD) has been developed, which decomposes the tensor as several low-rank block terms [21]. Xiong *et al.* introduced the rank-$(L, L, 1)$ block term decomposition to characterize the HSI, where each block of the rank-$(L, L, 1)$ BTD is the outer product of a matrix and a vector [22]. Rank-$(L, L, 1)$ BTD is the degradation of the rank-$(L, M, N)$ BTD for trading the efficiency [21], resulting in inaccurate representation for each component.

In this paper, we develop a sparsity regularized rank-$(L, M, N)$ block term decomposition (named SR-BTD) to fully exploit multiple components of the HSI. As shown in Figure 1, in SR-BTD, the clean HSI is decomposed as a sum of multiple components, where each component is a sparse core tensor multiplied by matrices along each mode. The requirement of sparsity on each core tensor can benefit determining the low-rankness of each component with the unknown rank-$(L, M, N)$ in the real world, leading to more accurately exploiting each component. Equipped with SR-BTD, we establish the HSI denoising model. To efficiently solve the resulting rank-$(L, M, N)$ BTD-based model, we design a hierarchical alternating least squares-based algorithm, where the computing of the rank-$(L, M, N)$ BTD is divided as several rank-$(L, M, N)$ approximation subproblems with cheap computational cost instead of requiring the closed-form solution with a heavy computational burden.

The main contributions of this work are two folds:

(1) We develop a sparsity regularized rank-$(L, M, N)$ block term decomposition (named SR-BTD), which can fully and accurately exploit multiple components of the HSI with the unknown rank-$(L, M, N)$ in the real world.

(1) Equipped with SR-BTD, we establish the HSI denoising model and design a hierarchical alternating least squares-based algorithm to efficiently solve the resulting model. Extensive experiments on simulated and real HSI denoising demonstrate SR-BTD is superior to the competing methods in terms of numerical results and visual quality.

## 2. NOTATIONS AND PRELIMINARIES

Here we give notations and preliminaries for developing our model. Some common symbols used in this paper are provided in Table 1 [21].

***Definition* 1 (Rank-$(L, M, N)$ BTD [21])** *For a tensor $\mathcal{X} \in \mathbb{R}^{I\times J\times K}$, rank-$(L, M, N)$ BTD decomposes $\mathcal{X}$ into the sum of several terms, i.e.,*

$$\mathcal{X} = \sum_{r=1}^{R} \mathcal{D}_r \times_1 \boldsymbol{A}_r \times_2 \boldsymbol{B}_r \times_3 \boldsymbol{C}_r, \tag{1}$$

*where $\mathcal{D}_r$ is the core tensor of size $L \times M \times N$, $\boldsymbol{A}_r$ is a matrix of size $I \times L$ ($I \geq L$) with $\boldsymbol{A}_r^\top \boldsymbol{A}_r = \boldsymbol{I}_L$, $\boldsymbol{B}_r$ is a matrix of size $J \times M$ ($J \geq M$) with $\boldsymbol{B}_r^\top \boldsymbol{B}_r = \boldsymbol{I}_M$, $\boldsymbol{C}_r$ is a matrix of the size $K \times N$ ($K \geq N$) with $\boldsymbol{C}_r^\top \boldsymbol{C}_r = \boldsymbol{I}_K$, and $R$ is the number of terms.*

**Table 1**: Basic notations.

| Notations | Explanation |
|---|---|
| $x, \boldsymbol{x}, \boldsymbol{X}, \mathcal{X}$ | scalar, vector, matrix, tensor |
| $x_{ijk}$ | the $\{i, j, k\}$-th element of $\mathcal{X}$ |
| $\|\|\mathcal{X}\|\|_F$ | $\|\|\mathcal{X}\|\|_F = \sqrt{\sum_{ijk} x_{ijk}^2}$ |
| $\|\|\mathcal{X}\|\|_1$ | $\|\|\mathcal{X}\|\|_1 = \sum_{ijk} \|x_{ijk}\|$ |
| $\boldsymbol{X}^\top$ | transpose of $\boldsymbol{X}$ |
| $\boldsymbol{I}_n$ | identity matrix with size $n \times n$ |
| $\times_k$ | mode-$k$ tensor-matrix product |

## 3. METHOD

### 3.1. The proposed model

To fully exploit multiple components of the HSI, we develop a sparsity regularized rank-$(L, M, N)$ block term decomposition (SR-BTD) and establish the corresponding HSI denoising model. By equation (1), we have the following relationship, i.e.,

$$\mathcal{X}_r = \mathcal{D}_r \times_1 \boldsymbol{A}_r \times_2 \boldsymbol{B}_r \times_3 \boldsymbol{C}_r, \tag{2}$$

where $\mathcal{X}_r = \mathcal{X} - \sum_{j=1, j\neq r}^{R} \mathcal{D}_j \times_1 \boldsymbol{A}_j \times_2 \boldsymbol{B}_j \times_3 \boldsymbol{C}_j$ and $r = 1, 2, \ldots, R$. Introducing sparse regularization on each core tensor $\mathcal{D}_r$, we can establish the SR-BTD-based HSI denoising model, i.e.,

$$\begin{aligned} \min_{\substack{\mathcal{X},\mathcal{S},\mathcal{D}_r,\\ \boldsymbol{A}_r,\boldsymbol{B}_r,\boldsymbol{C}_r}} \; & \|\mathcal{S}\|_1 + \sum_{r=1}^{R} \tau_r \|\mathcal{D}_r\|_1 + \frac{\beta}{2}\|\mathcal{Y} - \mathcal{X} - \mathcal{S}\|_F^2 \\ & + \frac{\gamma}{2}\sum_{r=1}^{R} \|\mathcal{X}_r - \mathcal{D}_r \times_1 \boldsymbol{A}_r \times_2 \boldsymbol{B}_r \times_3 \boldsymbol{C}_r\|_F^2, \\ \text{s.t.} \; & \boldsymbol{A}_r^\top \boldsymbol{A}_r = \boldsymbol{I}_L, \boldsymbol{B}_r^\top \boldsymbol{B}_r = \boldsymbol{I}_M, \boldsymbol{C}_r^\top \boldsymbol{C}_r = \boldsymbol{I}_N, \end{aligned} \tag{3}$$

where $\mathcal{Y}$ is the observed HSI, $\mathcal{X}$ is the clean HSI, $\mathcal{S}$ is the sparse noise, $\tau_r$ ($r = 1, 2, \ldots, R$) are the balance parameters, and $\beta$ and $\gamma$ are penalty parameters.

### 3.2. The proposed algorithm

To efficiently solve the proposed model, we design the hierarchical alternating least squares (HALS)-based algorithm. At each iteration of the HALS-based algorithm, a single block of variables is updated, while the remaining variables are fixed.

• Update $\boldsymbol{A}_r$, $\boldsymbol{B}_r$, and $\boldsymbol{C}_r$: This subproblem is a rank-$(L, M, N)$ approximation, i.e.,

$$\begin{aligned} \min_{\boldsymbol{A}_r,\boldsymbol{B}_r,\boldsymbol{C}_r} \; & \frac{\gamma}{2}\|\mathcal{X}_r^t - \mathcal{D}_r^t \times_1 \boldsymbol{A}_r \times_2 \boldsymbol{B}_r \times_3 \boldsymbol{C}_r\|_F^2, \\ \text{s.t.} \; & \boldsymbol{A}_r^\top \boldsymbol{A}_r = \boldsymbol{I}_L, \boldsymbol{B}_r^\top \boldsymbol{B}_r = \boldsymbol{I}_M, \boldsymbol{C}_r^\top \boldsymbol{C}_r = \boldsymbol{I}_N, \end{aligned} \tag{4}$$

**Algorithm 1** HALS algorithm for solving the proposed model.

**Input** The observed $\mathcal{Y} \in \mathbb{R}^{I\times J\times K}$, $R$, $\tau_r$, $\beta$, $\gamma$, $L$, $M$, and $N$
**Initialize** $\mathcal{X}^0$, $\mathcal{S}^0$, $\mathcal{D}_r^0$, $\boldsymbol{A}_r^0$, $\boldsymbol{B}_r^0$, and $\boldsymbol{C}_r^0$.
**While** not converged and $t \leq 200$ **do**
Update $\boldsymbol{A}_r^{t+1}$, $\boldsymbol{B}_r^{t+1}$, and $\boldsymbol{C}_r^{t+1}$ via (4).
Update $\mathcal{D}_r^{t+1}$ via (5).
Update $\mathcal{X}^{t+1}$ via (6).
Update $\mathcal{S}^{t+1}$ and via (7).
Update $\beta = 1.2 * \beta$ and $\gamma = 1.2 * \gamma$.
Let $t = t + 1$.
Check the stopping condition:
$\|\mathcal{X}^{t+1} - \mathcal{X}^t\|_F^2 / \|\mathcal{X}^t\|_F^2 \leq 10^{-6}$ or $t > 200$.
**End while**

where $\mathcal{X}_r^t = \mathcal{X} - \sum_{j=1}^{r-1} \mathcal{D}_j^{t+1} \times_1 \boldsymbol{A}_j^{t+1} \times_2 \boldsymbol{B}_j^{t+1} \times_3 \boldsymbol{C}_j^{t+1} - \sum_{j=r+1}^{R} \mathcal{D}_j^t \times_1 \boldsymbol{A}_j^t \times_2 \boldsymbol{B}_j^t \times_3 \boldsymbol{C}_j^t$ and $r = 1, 2, \ldots, R$. $\boldsymbol{A}_r^{t+1}, \boldsymbol{B}_r^{t+1}, \boldsymbol{C}_r^{t+1}$ can be updated by HOSVD [23].

• Update $\boldsymbol{D}_r$: Due to $\boldsymbol{A}_r^{t+1}$, $\boldsymbol{B}_r^{t+1}$, and $\boldsymbol{C}_r^{t+1}$ are semi-orthogonal, this subproblem can be solved by the soft thresholding operator, i.e.,

$$\mathcal{D}_r^{t+1} = \texttt{Soft}\left(\mathcal{X}_r^t \times_1 \boldsymbol{A}_r^{t+1\top} \times_2 \boldsymbol{B}_r^{t+1\top} \times_3 \boldsymbol{C}_r^{t+1\top}, \frac{\tau_r}{\gamma}\right). \tag{5}$$

• Update $\mathcal{X}$: This subproblem is a least-square problem and can be solved as

$$\mathcal{X}^{t+1} = \frac{\gamma \sum_{r=1}^{R} \mathcal{X}_r^{t+1} + \beta(\mathcal{Y} - \mathcal{S}^t)}{\beta + \gamma}, \tag{6}$$

where $\mathcal{X}_r^{t+1} = \mathcal{D}_r \times_1 \boldsymbol{A}_r^{t+1} \times_2 \boldsymbol{B}_r^{t+1} \times_3 \boldsymbol{C}_r^{t+1}$.

• Update $\mathcal{S}$: This subproblem can be solved by the soft thresholding operator, i.e.,

$$\mathcal{S}^{t+1} = \texttt{Soft}\left(\mathcal{Y} - \mathcal{X}^{t+1}, \frac{1}{\gamma}\right). \tag{7}$$

We summarize the solving algorithm in **Algorithm** 1.

## 4. EXPERIMENTS

To evaluate the performance of SR-BTD, we conduct experiments on simulated and real noisy hyperspectral images. The compared methods include Tucker decomposition-based LRTA [12], TSVD-based LRTR [17], 3DTSVD-based 3DTNN [20], and rank-$(L, L, 1)$ BTD-based RSLRNTF [22], which only consider exploiting the low-rank prior by different tensor decomposition.

### 4.1. Simulated data

Pavia City Center[1] $(200 \times 200 \times 80)$ is tested in the this experiment. The clean image is normalized to [0, 1] band-wisely.

[1] http://lesun.weebly.com/hyperspectral-data-set.html

**Table 2**: The numerical results of all compared methods on Pavia City Center. Boldface highlights the **best** values.

| | Metrics | Noisy | LRTA | LRTR | 3DTNN | RSLRNTF | SR-BTD |
|---|---|---|---|---|---|---|---|
| Case 1 | MPSNR | 17.28 | 20.42 | 28.31 | 30.68 | 29.74 | **31.48** |
| | MSSIM | 0.2890 | 0.478 | 0.8332 | 0.9015 | 0.8767 | **0.9026** |
| | SAM | 31.056 | 17.66 | 7.047 | 4.898 | 5.861 | **4.673** |
| | Time (s) | - | 2.745 | 51.868 | 79.160 | 69.503 | 68.862 |
| Case 2 | MPSNR | 10.16 | 19.91 | 24.94 | 29.32 | 24.58 | **29.86** |
| | MSSIM | 0.0726 | 0.4825 | 0.6474 | 0.8566 | 0.7596 | **0.8689** |
| | SAM | 44.627 | 9.284 | 7.798 | 5.613 | 6.358 | **5.153** |
| | Time (s) | - | 2.681 | 24.855 | 78.691 | 69.990 | 67.945 |

The mean value of the peak signal-to-noise ratio of each band (MPSNR), the mean value of structural similarity index of each band (MSSIM), and the spectral angle mapping (SAM) are employed as three metrics.

Two simulated noise cases are set as follows:

*Case 1 Gaussian noise + stripes + deadlines:* The zero-mean Gaussian noise is added, and the noise deviations are randomly selected within the interval of $[0.1, 0.2]$ for each band. 10 bands are randomly selected and each band is corrupted by 20 stripes. 10 bands are randomly selected and each band is corrupted by 10 deadlines.

*Case 2 Gaussian noise + impulse noise:* The zero-mean Gaussian noise is added, and the noise deviations are randomly selected within the interval of $[0.1, 0.2]$ for each band. Then, the impulse noise is added to all bands, where the percentage of polluted pixels is set as $0.3$ for each band.

Table 2 lists MPSNR, MSSIM, and SAM values for numerical comparison. As observed, the numerical results of SR-BTD are superior to those of the compared methods. Figure 2 shows the visual results by different methods in case 1. From Figure 2, we can find that SR-BTD removes almost all of the noise, especially stripes and deadlines. As compared with rank-$(L, L, 1)$ BTD-based RSLRNTF, SR-BTD preserves the color fidelity. The reason is that SR-BTD can more fully and accurately exploit the multiple components of the HSI.

### 4.2. Real data

WHU-Hi-HongHu Data, which contains $940 \times 475$ pixels and 270 bands, is used in this experiment. A $256 \times 256 \times 270$ subimage of this data is used to test. As there is no reference clean HSI, we show the visual results by different methods in Figure 3. We can observe that SR-BTD successfully removes almost all of the noise and preserves more details as compared with other tensor decompositions. This improvement is attributed that SR-BTD can fully and accurately exploit the multiple components of the HSI.


**Fig. 2**: The pseudo-color recovered results (RGB: Bands 62, 36, 1) of Pavia City Center by different methods in case 1.

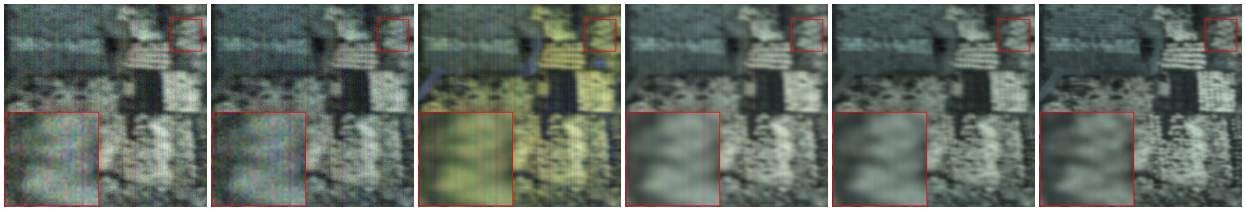


**Fig. 3**: The pseudo-color recovered results (RGB: Bands 246, 259, 270) of WHU-Hi-HongHu Data by different methods.

## 5. CONCLUSION

In this paper, we developed an SR-BTD decomposition to fully exploit the multiple components of the HSI. Equipped with SR-BTD, we established the HSI denoising model and designed a HALS-based algorithm to efficiently solve the resulting model. Extensive experiments on simulated and real HSI denoising tasks demonstrated SR-BTD is superior to the competing tensor decompositions.

## REFERENCES


[1] Z. Zhang, E. Pasolli, M. M. Crawford, and J. C. Tilton, "An active learning framework for hyperspectral image classification using hierarchical segmentation," *IEEE J. Sel. Topics Appl. Earth Observ. Remote Sens.*, vol. 9, no. 2, pp. 640–654, 2016.

[2] J. Ma, H. Zhou, J. Zhao, Y. Gao, J. Jiang, and J. Tian, "Robust feature matching for remote sensing image registration via locally linear transforming," *IEEE Trans. Geosci. Remote Sens.*, vol. 53, no. 12, pp. 6469–6481, 2015.

[3] M. Zhang, W. Li, R. Tao, H. Li, and Q. Du, "Information fusion for classification of hyperspectral and lidar data using IP-CNN," *IEEE Trans. Geosci. Remote Sens.*, vol. 60, pp. 1–12, 2022, Art no. 5506812.

[4] J. Liu and J. Zhang, "Spectral unmixing via compressive sensing," *IEEE Trans. Geosci. Remote Sens.*, vol. 52, no. 11, pp. 7099–7110, 2014.

[5] K. Wei, Y. Fu, and H. Huang, "3-D quasi-recurrent neural network for hyperspectral image denoising," *IEEE Trans. Neural Netw. Learn. Syst.*, vol. 32, no. 1, pp. 363–375, 2021.

[6] L. Zhuang, L. Gao, B. Zhang, X. Fu, and J. M. Bioucas-Dias, "Hyperspectral image denoising and anomaly detection based on low-rank and sparse representations," *IEEE Trans. Geosci. Remote Sens.*, vol. 60, pp. 1–17, 2022, Art no. 5500117.

[7] H. Zhang, W. He, L. Zhang, H. Shen, and Q. Yuan, "Hyperspectral image restoration using low-rank matrix recovery," *IEEE Trans. Geosci. Remote Sens.*, vol. 52, no. 8, pp. 4729–4743, 2014.

[8] Y. Chen, Y. Guo, Y. Wang, D. Wang, C. Peng, and G. He, "Denoising of hyperspectral images using nonconvex low rank matrix approximation," *IEEE Trans. Geosci. Remote Sens.*, vol. 55, no. 9, pp. 5366–5380, 2017.

[9] Y. Xie, Y. Qu, D. Tao, W. Wu, Q. Yuan, and W. Zhang, "Hyperspectral image restoration via iteratively regularized weighted Schatten $p$-norm minimization," *IEEE Trans. Geosci. Remote Sens.*, vol. 54, no. 8, pp. 4642–4659, 2016.

[10] L. Zhuang and J. M. Bioucas-Dias, "Fast hyperspectral image denoising based on low rank and sparse representations," *IEEE J. Sel. Topics Appl. Earth Observ. Remote Sens.*, vol. 11, no. 3, pp. 730–742, 2018.

[11] H. Zeng, Y. Chen, X. Xie, and J. Ning, "Enhanced nonconvex low-rank approximation of tensor multi-modes for tensor completion," *IEEE Trans. Comput. Imaging*, vol. 7, pp. 164–177, 2021.

[12] N. Renard, S. Bourennane, and J. Blanc-Talon, "Denoising and dimensionality reduction using multilinear tools for hyperspectral images," *IEEE Geosci. Remote Sens. Lett.*, vol. 5, no. 2, pp. 138–142, 2008.

[13] A. Karami, M. Yazdi, and A. Z. Asli, "Noise reduction of hyperspectral images using kernel non-negative tucker decomposition," *IEEE J. Sel. Topics Signal Process.*, vol. 46, no. 7, pp. 487–493, 2011.

[14] Y. Wang, J. Peng, Q. Zhao, Y. Leung, X.-L. Zhao, and D. Meng, "Hyperspectral image restoration via total variation regularized low-rank tensor decomposition," *IEEE J. Sel. Topics Appl. Earth Observ. Remote Sens.*, vol. 11, no. 4, pp. 1227–1243, 2018.

[15] I. V. Oseledets, "Tensor-train decomposition," *SIAM J. Sci. Comput.*, vol. 33, pp. 2295–2317, 2011.

[16] A. Cichocki, N. Lee, I. Oseledets, A. Phan, Z. Q, and D. P. Mandic, "Tensor networks for dimensionality reduction and large-scale optimization: Part 1 low-rank tensor decompositions," *Found. Trends Mach. Learn.*, vol. 9, pp. 249–429, 2016.

[17] H. Fan, Y. Chen, Y. Guo, H. Zhang, and G. Kuang, "Hyperspectral image restoration using low-rank tensor recovery," *IEEE J. Sel. Topics Appl. Earth Observ. Remote Sens.*, vol. 10, no. 10, pp. 4589–4604, 2017.

[18] M. E. Kilmer, L. Horesh, H. Avron, and E. Newman, "Tensor-tensor algebra for optimal representation and compression of multiway data," *Proc. Natl. Acad. Sci. U.S.A.*, vol. 118, p. e2015851118, 2021.

[19] H. Fan, C. Li, Y. Guo, G. Kuang, and J. Ma, "Spatial-spectral total variation regularized low-rank tensor decomposition for hyperspectral image denoising," *IEEE Trans. Geosci. Remote Sens.*, vol. 56, no. 10, pp. 6196–6213, 2018.

[20] Y.-B. Zheng, T.-Z. Huang, X.-L. Zhao, T.-X. Jiang, T.-H. Ma, and T.-Y. Ji, "Mixed noise removal in hyperspectral image via low-fibered-rank regularization," *IEEE Trans. Geosci. Remote Sens.*, vol. 58, no. 1, pp. 734–749, 2020.

[21] L. D. Lathauwer, "Decompositions of a higher-order tensor in block terms—Part II: Definitions and uniqueness," *SIAM J. Matrix Anal. Appl.*, vol. 30, no. 3, pp. 1033–1066, 2008.

[22] F. Xiong, J. Zhou, and Y. Qian, "Hyperspectral imagery denoising via reweighed sparse low-rank nonnegative tensor factorization," in *Proc. IEEE Int. Conf. Image Process. (ICIP)*, 2018, pp. 3219–3233.

[23] L. D. Lathauwer, B. D. Moor, and J. Vandewalle, "A multilinear singular value decomposition," *SIAM J. Matrix Anal. Appl.*, vol. 21, no. 4, pp. 1253–1278, 2000.